Proceedings of ASME Turbo Expo 2025
Turbomachinery Technical Conference and Exposition
GT2025
June 16-20, 2025, Memphis, Tennessee

GT2025-153376

MODULATION OF THE THICKENED FLAME MODEL INTO EDDY DISSIPATION CONCEPT FOR MULTI-REGIME COMBUSTION MODELLING

R. Meloni
Baker Hughes
Florence, Italy
Email: *roberto.meloni@bakerhughes.com*.

N. Ansari, S. Orsino, F. Reza
Ansys Inc
Canonsburg, USA

S. Castellani, G. Lemmi, A. Andreini
Department of Industrial Engineering
University of Florence,
Florence, Italy

ABSTRACT

The modelling of multi-regime turbulent flames is a challenging topic, especially when dealing with industrial burner designs under modern gas turbine conditions. Unfortunately, neither the reduced order combustion models (relying on the tabulated chemistry concept) nor the most computationally expensive ones (based on the species transport) are always predictive in describing the flame front characteristics. In the former approach, the tabulation of premixed or non-premixed flamelets is typically decided a priori, thus making the description of the multi-regime combustion process daring. On the other side, species transport-based turbulent combustion models are characterized by higher flexibility and do not have significant limitations. However, some of them are strictly valid only for specific combustion regimes: for instance, the Thickened Flame Model (TFM) is formally suitable only in the context of premixed combustion.

In this work, in the framework of the species transport model, a novel hybrid closure is proposed: while the premixed part relies on the TFM, the non-premixed one is modelled using the well-known Eddy Dissipation Concept (EDC). The mathematical formulation as well as the validation of the approach against the experimental data – retrieved at atmospheric pressure and high oxidizer temperature of an industrial burner – will be presented.

Keywords*:* Multi Regime Combustion, Thickened Flame Model, Eddy Dissipation Concept, Computational Fluid Dynamics.

NOMENCLATURE

Roman letters

D	Species diffusivity	[m^2 s^{-1}]
E	Efficiency function	[-]
F	Thickening factor	[-]
N	Number of points in the flame front	[-]
Y	Mass fraction	[-]
Z	Mixture fraction	[-]

Greek

α	Efficiency function constant	[-]
φ	Vector of the species mass fractions	[-]
Φ	Equivalence ratio	[-]
Γ	Efficiency function parameter	[-]
ξ	EDC model parameter	[-]
κ	Fine scales' volume fraction	[-]
∇	Gradient operator	
Δ	Divergence operator	
Ω	Flame sensor	[-]
ρ	Density	[kg m^{-3}]
τ	Computational/Characteristic time	[s]
$\dot{\omega}$	Reaction Rate	[kg m^3 s^{-1}]

Subscripts and Superscript

f	Referred to fuel
ox	Referred to oxidant
l	Laminar quantity
t	Turbulent quantity
max	Referred to the thickening factor
sgs	Sub-grid scale quantity

Acronyms

CFD	Computational Fluid Dynamics
EDC	Eddy Dissipation Concept

FI	Flame Index
FR	Finite Rate
FTT	Flow Through Time
GT	Gas Turbine
HRR	Heat Release Rate
LES	Large Eddy Simulation
LFS	Laminar Flame Speed
LFT	Laminar Flame Thickness
ORZ	Outer Recirculation Zone
PIV	Particle Image Velocimetry
TCI	Turbulence Chamistry Interaction
TFM	Thickened Flame Model
THT	Techonology for High Temperature
UDF	User Defined Function
WALE	Wall Adaptive Local Eddy-viscosity

1. INTRODUCTION

The challenges that GT manufacturers have to face in the design phase of a combustion system require the employment of the most accurate numerical analysis to support any decision. The interaction between turbulent flow and chemical reactions as well as the proper characterization of the flame brush represent the main aspects that modern Computational Fluid Dynamics (CFD) codes are asked to properly describe for the improvement of the hardware, having as the ultimate goal the abatement of the pollutant emissions and the extension of the durability of the hot gas path components [1-4].

A reliable numerical prediction of the main features of the heat release region can be very challenging, especially when dealing with industrial geometries, whose operating conditions are characterized by high Reynolds numbers across different operating modes [5-6]. As a primary consequence, the CFD analysis could be very demanding from a computational standpoint. Pre-tabulated chemistry models found their popularity thanks to a strong decoupling of the combustion problem from the rest of the numerical solution leading to a huge reduction of the effort and the *time-to-solution*. Conversely, some of the hypotheses that these models are founded on may result in important limitations in the physical description of the flame brush. The flamelet assumption not only intrinsically neglects the impact of the stretch and the heat loss on the velocity at which the reaction proceeds but also the impact on the species concentrations is not accounted for, unless dedicated customizations are embedded in the code [7-8]. Such defects are even more significant when the system is characterized by a multi-regime combustion process. Very few models relying on the pre-tabulated approach nowadays published in the literature are able to span from fully premixed to non-premixed regimes within a single time-step of a given design [9]. Most of the time, the user must decide *a-priori* the kind of tabulation by which the system has to be described, accepting an error in those regions where a different combustion regime takes place.

On the other hand, combustion models relying on the direct transport of species and chemical reactions are intrinsically able to account for the effect on the flame of all the above-mentioned phenomena, even if the rise of the computational cost makes this strategy almost unaffordable in the context of highly turbulent systems. This is particularly true when the employed chemistry is described not by a single or two-step scheme, but by a detailed or even a skeletal mechanism. Some of the species transport combustion models like the EDC [10] can be adopted to simulate a combustor with a multi-combustion regime. Others, like the Thickened Flame Model (TFM) [11-12], are optimized in the simulation of fully-premixed or partially premixed mixtures while they are not recommended for non-premixed regimes [13].

Recently, different research groups implemented the same hybridization of the TFM: based on the local value of a flame index able to provide information on the combustion regime taking place, the mathematical closure of the transport equations is left unaltered for the premixed regime while the Finite Rate (FR) approach is adopted for the non-premixed one. In this way, the TFM can be extended also to the simulation of a mixed regime. Such a strategy is easy to implement along the TFM formulation since the FR closure is obtained by fixing the artificial thickening factor as well as the efficiency function to the unity [14]. The main drawback of this approach is that the turbulence-chemistry interaction (TCI) is completely suppressed. This can represent a more or less strong simplification. The degree of simplification depends strongly on the mesh resolution, time-step, and Reynolds number, which influences turbulence and flame morphology. For sufficiently refined simulations, approaching a DNS-like resolution, the omission of turbulence-chemistry interaction (TCI) has minimal impact. However, in high-Reynolds-number flows typical of industrial applications, where resolution constraints are more pronounced, the numerical solution can be significantly compromised [15]. Conversely, for low-Reynolds-number lab-scale systems, this approach often provides results in excellent agreement with experiments [16].

In the context of the TFM extension for multi-regime combustion, an interesting idea could be the coupling of this model with the EDC, the latter for the modelling of the non-premixed part only. The adoption of such a strategy allows for the use of the TFM as the best-in-class model for premixed combustion while introducing the proper TCI for the non-premixed regime through the EDC model. Overall, this approach can be seen as an attempt to optimize a numerical procedure for multi-regime combustion processes.

In this paper, the mathematical formulation aiming at accomplishing this target will be presented. In particular, the way the transport equations of the TFM are manipulated to be adapted to the EDC theory without altering the transport properties of the species will be deeply discussed, since it represents an innovative and non-trivial task. Moreover, a validation case will be investigated to measure the improvement of this strategy against the one without the inclusion of turbulence-chemistry interaction. Different aspects characterizing the flame morphology will be considered in this regard leveraging detailed experimental measurements. According to the Authors' knowledge, this is the first time such a methodology is presented in the open literature.

The manuscript will report the description of the mathematics in the next paragraph and the main feature of the test rig and the operating conditions in the following. The Results and Discussion section will provide a quantitative assessment of the improvement of the flame morphology prediction along the TFM-EDC model, especially for the prediction of the lift-off of the pilot flame through which the investigated burner is stabilized.

2. NUMERICAL MODELLING

2.1. Multi-Regime Combustion modelling: TFM-FR vs TFM-EDC formulation

The TFM mathematics represents the foundation for the combustion model extensions required to model the characteristics of both premixed and non-premixed regimes: the only difference between the two extensions concerns the way the transport equations of the generic species are modified to deal with non-premixed combustion regime. So, the premixed part remains unchanged and, according to the original formulation of the TFM proposed by Colin et al. [17], the transport equation of the species mass fraction φ can be written as:

$$\frac{\partial \bar{\rho}\, \tilde{\varphi}}{\partial t} + \frac{\partial \bar{\rho}\, \tilde{u}_j\, \tilde{\varphi}}{\partial x_j} = \frac{\partial}{\partial x_j}\left(\bar{\rho}(EFD_l + (1-\Omega)D_t)\frac{\partial \tilde{\varphi}}{\partial x_j}\right) + \frac{E}{F}\dot{\omega}(\tilde{\varphi}) \quad (1)$$

where E, F and Ω are the efficiency function, the dynamic thickening factor and the flame sensor, respectively. The efficiency function mimics the turbulence-chemistry interaction, partially recovering the weaker effect of the strain rate on an artificially thickened flame front. The latter is obtained multiplying the laminar flame thickness by F in order to resolve the flame front in a mesh suitable for a Large-Eddy Simulation (LES). Colin's efficiency function is used in this work from [17] and the corresponding formula is reported in Eq. 2, as follows:

$$E = \frac{1 + \alpha \Gamma_0 \dfrac{u'_{\Delta_e}}{s_l^0}}{1 + \alpha \Gamma_1 \dfrac{u'_{\Delta_e}}{s_l^0}} \quad (2)$$

The efficiency function depends on the dilatation-free velocity at the test filter u'_{Δ_e} calculated through Durand et al's formulation [18] to make this assessment easier along unstructured grid (Eq. 3):

$$u'_{\Delta_e} = c\Delta\left|\nabla \times \tilde{\boldsymbol{u}} - \nabla \times \hat{\tilde{\boldsymbol{u}}}\right| \quad (3)$$

Moreover, the laminar properties, i.e., the laminar flame speed and thickness, are the model's inputs which are required for the calculation of the efficiency function. At this scope, the Bilger's formula is applied to retrieve the mixture fraction according to the local elemental mass fraction [19]: this is possible since a skeletal mechanism made of 27 species and 116 reactions derived from the UCSD detailed chemistry [20] is used. The chemistry set is made to account for methane oxidation and ethane chemistry also, according to the fuel composition of the selected test condition. The procedure through which such reduced mechanism is obtained can be found in [21]. Once the mixture fraction Z is assessed, the laminar properties are calculated leveraging polynomials curve fit with the mixture fraction as independent variable which can be derived and pre-calculated using a freely propagating flame in Cantera [22].

The thickening factor F (Eq. 4) is implemented according to the dynamic formulation proposed by Wang et al. [23]:

$$F = \Omega(F_{max} - 1) + 1 \quad (4)$$

The idea behind this approach is that the thickening is applied only inside the flame front detected through the flame sensor Ω. The maximum thickening factor is instead a function of the mesh resolution Δx, the number of points N used to discretize the laminar flame thickness, set to 5 in the present work (Eq. 5):

$$F_{max} = \frac{\Delta x\, N}{LFT(Z)} \quad (5)$$

The reaction involving methane and radical OH ($index\ 42\colon CH_4 + OH <=> CH_3 + H_2O$) is used as flame front marker to calculate Ω, according to Eq. 6:

$$\Omega = \tanh\left(\beta \frac{|\overline{\dot{\omega}_{42}}|}{\max(|\overline{\dot{\omega}_{42}}|)}\right) \quad (6)$$

where β is a constant of the model and $\dot{\omega}_{42}$ the reaction rate of the reference reaction.

The above described approach is applied for positive values of a Flame Index (FI), calculated leveraging the gradients of fuel and oxygen to discriminate the combustion regime (Eq. 7):

$$FI = \frac{\nabla Y_F \cdot \nabla Y_{ox}}{|\nabla Y_F \cdot \nabla Y_{ox}|} \quad (7)$$

When the FI is negative, the species transport equation is modified according to the FR and the EDC model.

In the former case, as stated in the Introduction, both the Efficiency Function and the Thickening Factor are fixed to 1, meaning that the laminar closure is adopted and the TCI neglected. Inside the flame front the transport equations of the chemical species becomes:

$$\frac{\partial \bar{\rho}\, \tilde{\varphi}}{\partial t} + \frac{\partial \bar{\rho}\, \tilde{u}_j\, \tilde{\varphi}}{\partial x_j} = \frac{\partial}{\partial x_j}\left(\bar{\rho}(D_l + D_t)\frac{\partial \tilde{\varphi}}{\partial x_j}\right) + \dot{\omega}(\tilde{\varphi}) \quad (8)$$

Conversely, when the EDC closure is chosen, the first step is the verification of the local value of the FI: if it is negative, the species diffusivities are prevented from being altered leading to fixing the efficiency and the thickening factor to 1 (similar along the FR approach). Additionally, the source term of Eq. 1 is further customized by replacing E with what suggested by Magnussen et al. [10] in the fine-scales theory. In formula:

$$E \rightarrow k = \frac{\xi^{*2}}{1-\xi^{*3}} \tag{9}$$

With k identifying the volume fraction of the fine structures. In an LES context, the length scale (ξ^*) is computed as:

$$\xi^* = \sqrt{\frac{\tau_{kolmog}}{\tau_{sgs}}} \tag{10}$$

The Kolmogorov (τ_{kolmog}) and sub-grid scale turbulence (τ_{sgs}) time scales are calculated as:

$$\tau_{kolmog} = \sqrt{\frac{\mu}{\rho \cdot \sigma}} \tag{11}$$

$$\tau_{sgs} = \frac{l_{sgs}}{u'_{sgs}} \tag{12}$$

Here, μ is the molecular viscosity of the mixture, ρ the density, u'_{sgs} and l_{sgs} are the velocity fluctuation and the turbulent length scale at the sub-grid-scale, respectively, both depending on the specified sub-grid scale model, and σ the is the average rate of dissipation of turbulence kinetic energy per unit mass. In an LES context, σ is calculated as:

$$\sigma = \frac{{u'_{sgs}}^3}{l_{sgs}} \tag{13}$$

By definition, the volume fraction of the fine structures where the reactions are supposed to take place, leads to values of k always bounded between 0 and 1, mimicking in this way the turbulence-chemistry interaction.

In this work, the EDC time-scale is set equal to the solver time-step. It is important to note, as general information, that the chemistry integration time is independent of the EDC time-scale and is instead fixed to the solver time-step.

The approach proposed here can be generalized to adopt slightly different formulations of the non-premixed source term, like the fractal theory of the EDC [24,25] or even the Partially Stirred Reactor (PaSR). In this manuscript, only the basic formulation of the EDC is evaluated while the impact of the other formulations is left to future works.

The entire customization of the combustion model is based on the execution of a User Defined Function (UDF) implemented in the commercial code Ansys Fluent.

2.2. Computational Grid and Numerical Setting

The numerical grid represents a key point for a good prediction of the flame peculiarities. In multi-regime systems it must allow the combustion model to accurately describe both the premixed and non-premixed flame fronts. To accomplish this task and optimize the computational effort, different mesh resolutions are applied along the computational domain. The main components of the latter, such as the premixer, the dome plate and the quartz are reported in Figure 1. The other components like the upstream plenum, the premixer and the downstream flame tube are not reported in the picture. The details of the premixer design as well as of the pilot line are not reported for confidentiality reasons. In any case, the premixer is a double-counter rotating swirler ensuring a high degree of premixing of the fuel injected in cross flow through the blades [3-8]. The main flame produced by the stratified stream coming from the burner is dominantly premixed. On the other side, the flame stabilization is ensured by different pilots mounted all around the burner tip and injecting the fuel directly into the primary zone. The main characteristic of such pilot flames is their non negligible lift-off height that, increasing the mixing with the surrounding mixture allows to reach low NO_x emissions (< 15 ppmvd at ISO conditions).

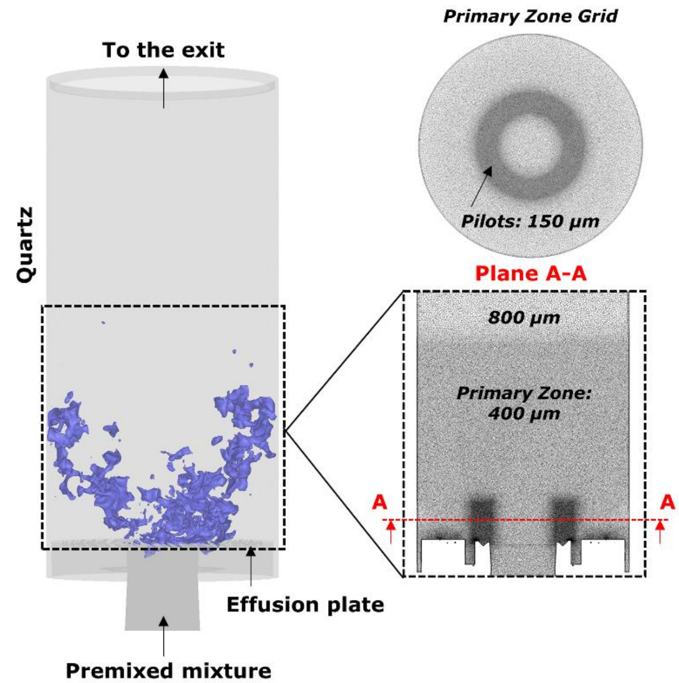

FIGURE 1: ASSEMBLY OF THE BURNER WITH THE QUARTZ FLAME TUBE THROUGH THE EFFUSION COOLING (LEFT) AND THE CORRESPONDING NUMERICAL GRID WITH A CLOSE-UP ON THE PRIMARY ZONE DISCRETIZATION (RIGHT)

Going back to the mesh resolutions, Figure 1 reports also the size of the grid along the main regions of the combustor. It can be seen that the primary zone is discretized with a mesh resolution of about 400 μm. As previously stated, here the premixed combustion regime is expected to be the main one. So, Eq. 5 can be used to calculate this number considering the laminar flame thickness at the simulated operating conditions and a maximum thickening factor of around 6. An even more refined mesh is applied inside the pilot fuel line and in a cylindric volume inside the primary zone where the pilot fuel enters into the combustor. Here the resolution goes down to 150 μm since the expected non-premixed regime requires finer mesh to correctly capture the mixing among reactants. The remaining portions of the computational domains employ coarse mesh discretization, close to 800 μm or even higher. The total number of polyhedral elements is 24 million. Such mesh discretization is similar to the one employed in [15] where it is demonstrated its ability in correctly predict the flow field main features as well as the majority of the turbulent scales. Based on those findings, here no mesh sensitivity will be reported.

A mass flow rate type boundary condition is adopted for all the inlets in the domain and specifically for the premixed and pilot fuel lines, the combustion air and also the air passing through the dome cooling it by effusion. A dedicated flow network is leveraged to calculate the air split among the passages of the rig knowing their effective area: this calculation includes also the air that doesn't participate in the combustion process and cool down the quartz passing through the gap between the quartz itself and the external casing. This big portion of the rig is not included in the model to save elements. In any case, knowing the correspondent mass flow rate, an external convective heat transfer coefficient has been assessed by correlation and applied as thermal boundary condition (together with the thickness of the quartz and the temperature of the coolant) to quantify the heat loss through the quartz. The thermal boundary condition for the dome plate and the burner tip are retrieved from the temperature measured by dedicated thermocouples. The outlet is modelled through a standard pressure outlet type boundary condition.

Regarding the turbulence setting, the WALE scheme is adopted to model the sub-grid scale part of the LES while all the equations are resolved at the second discretization order. The solution strategy consists of 4 Flow Through Times (FTT) simulated to wash-out the RANS initialization and additional 4 FTTs to retrieve the time-averaged solution.

3. TEST RIG AND OPERATING CONDITION

The atmospheric test rig at the THT lab is employed to execute the experimental test campaign. Figure 2 shows the hot section of the rig with its most relevant features. The burner is installed inside a plenum from which the air splits into the above mentioned main streams: the combustion air passing through the premixer, the effusion cooling of the dome and the cooling flow of the liner. The external casing is provided with orthogonal windows allowing the visualization of the quartz and, consequently, the characterization of what happens inside the primary zone. Thanks to this optical access, both the flow filed through the PIV and the heat release rate via the chemiluminescence can be performed.

At this regard, the flame images are recorded coupling an intensifier equipped with a bandpass filter with a Phantom MIRO 340 camera. The OH^{*} filter (±310 nm) is employed for the test conditions under investigation; unfortunately, no comparison between the OH^{*} and the CH^{*} filter is available. The images are recorded with a frequency of 500 Hz, an exposure time of 0.5 ms

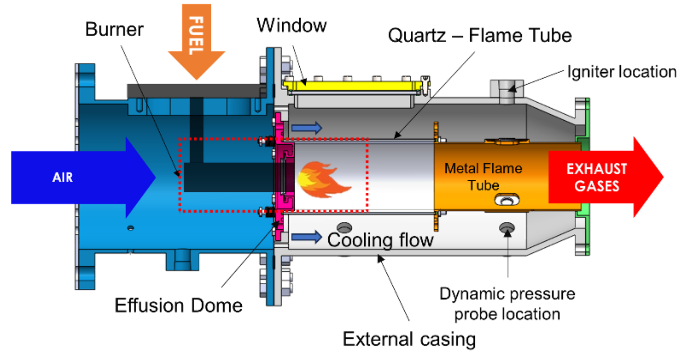

FIGURE 2: HOT SECTION OF THE THT RIG FROM THE OXIDIZER PLENUM UP TO THE EXHAUST GAS SECTION

and a gain of 5. The quartz is fixed to the dome and to the downstream metal flame tube. The latter is equipped with:

a) a dynamic pressure probe for the detection of thermo-acoustic instabilities;
b) an igniter;
c) thermocouples at 3 different axial locations;
d) a sampling probe through which the exhaust gases are extracted from the combustor and sent to a HORIBA PG300 for the analysis of the pollutant emissions (NO_x, CO) and the residual oxygen.

No additional information about the auxiliary systems of the article (fuel gas, electric heater, etc.) are provided here for sake of brevity. More information about that can be found in [26].

The main data characterizing the simulated test condition are summarized in Table 1. The air has a temperature of about 576 K that is relevant for a GT cycle. The total air mass flow rate elaborated by the compressor (320 g/s) is such that the pressure drop across the burner (measured through dedicated probes) is in line with the values this design is used to work with. Regarding the fuel, its composition is characterized by a non-negligible amount of ethane (~7%) that forced its inclusion in the skeletal mechanism. The fuel split is equal to 35% meaning that the pilot fuel line and the main one provide 35% and 65% of the total thermal power, respectively. The latter is equal to 75 kW.

TABLE 1: SELECTED OPERATING CONDITIONS OF THE TEST ARTICLE

Air		
Temperature	[K]	576
Total mass flow rate	[g/s]	320
Fuel		
Gas composition	92% CH_4, 7% C_2H_6, 1% inert	
Temperature	[K]	330
Pilot Split	[%]	35
Operating pressure	[bar]	1.016
Thermal Power	[kW]	75

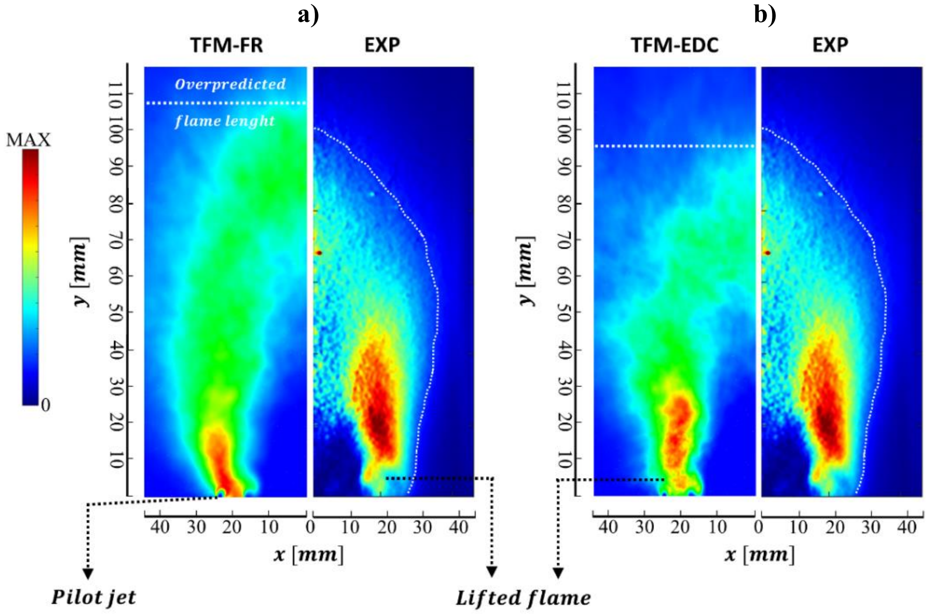

FIGURE 3: COMPARISON BETWEEN THE ABEL-TRANSFORMED OH FROM THE EXPERIMENTS AND THE HRR FOR THE TFM-FR CLOSURE (a) AND THE TFM-EDC (b)

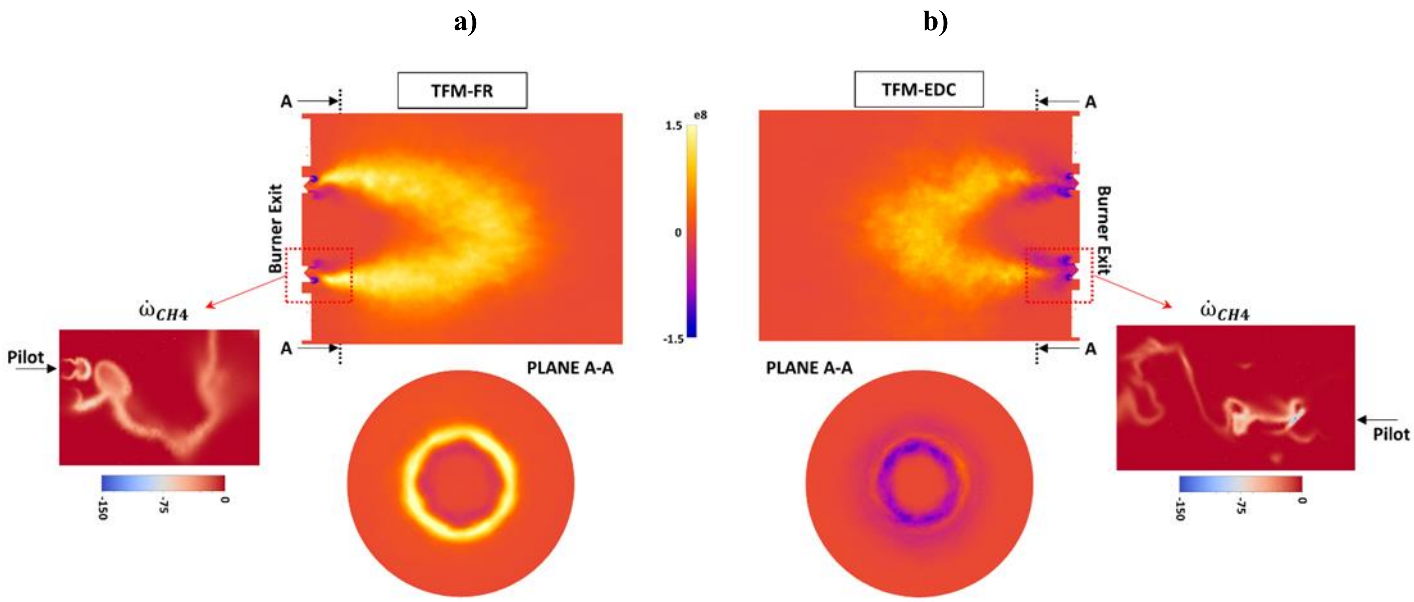

FIGURE 4: HRR CONDITIONED BY THE FI FOR THE TFM-FR (a) AND THE TFM-EDC (b) MODEL. THE MAGNIFIED CONTOUR PLOTS CLOSE TO ONE OF THE PILOT JET EXITS SHOW THE METHANE CONSUMPTION RATE

4. RESULTS AND DISCUSSION

This section will be divided into two sub-paragraphs where the different mathematical closures for the transport equations are compared: the first aiming at the flame characterization, the second quantifying the differences in terms of flow field leveraging PIV measures.

4.1. Flame Morphology Results

Figure 3 summarizes the comparison between the two numerical approaches and the experimental one. The latter is represented through the Abel-transformed of the OH^* time average field while the numerical ones by the time-average of the heat-release rate plotted on the longitudinal plane of the combustor.

From an experimental standpoint, the flame is characterized by a non-negligible lift-off of the pilots that can be quantified in around 8-10 mm from pilot exit, with the OH^* intensity peak located at around 20 mm. The heat release associated to the premixed mixture coming from the burner produces a much less intense flame and leading to a total flame length close to 100 mm from the burner exit. Such measure is calculated considering the maximum distance of the iso-line at 5% of the OH^* peak along the symmetry axis of the flame tube.

The $TFM - FR$ approach (Figure 3-a) has two major drawbacks, one related to the pilot and one to the premixed flame. The numerical solution doesn't show any lift-off of the pilots. On the contrary, the fuel jets start to be oxidized right after they enter inside the combustor leading to a HRR peak located a few millimeters downstream. Regarding the main, the opposite finding is achieved: the HRR map reveals a quite longer flame compared to the experiments. Figure 3-b reports the results of the $TFM - EDC$ closure: the inclusion of the TCI for the non-premixed combustion regime leads to a more accurate prediction of the experimental flame morphology. First of all, despite not completely captured, the pilot lift-off is much better reproduced. Moving from the burner exit, the HRR^* rises more gradually than in the FR closure producing a peak at approximately the same location of the experiments. Also, the morphology of the region at the highest OH^* intensity seems to be reproduced with a higher accuracy compared to the FR. Analogously, even the total flame

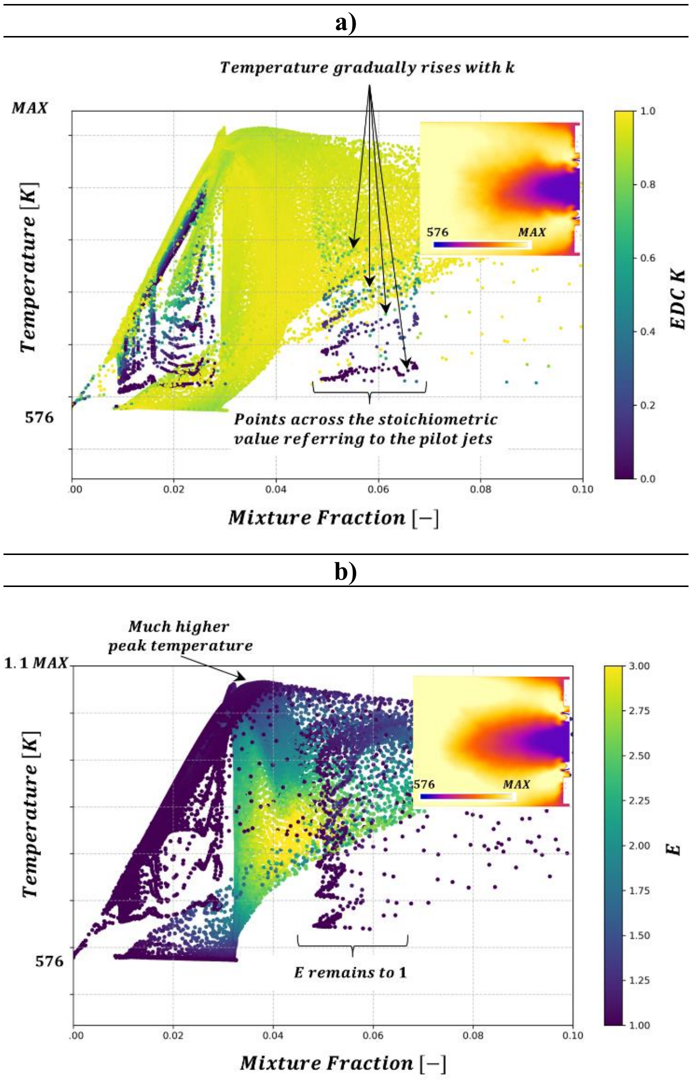

FIGURE 5: TEMPERATURE AS A FUNCTION OF THE MEAN MIXTURE FRACTION COLOURED BY k FOR TFM-EDC (a) AND BY THE EFFICIENCY FUNCTION FOR TFM-FR (b)

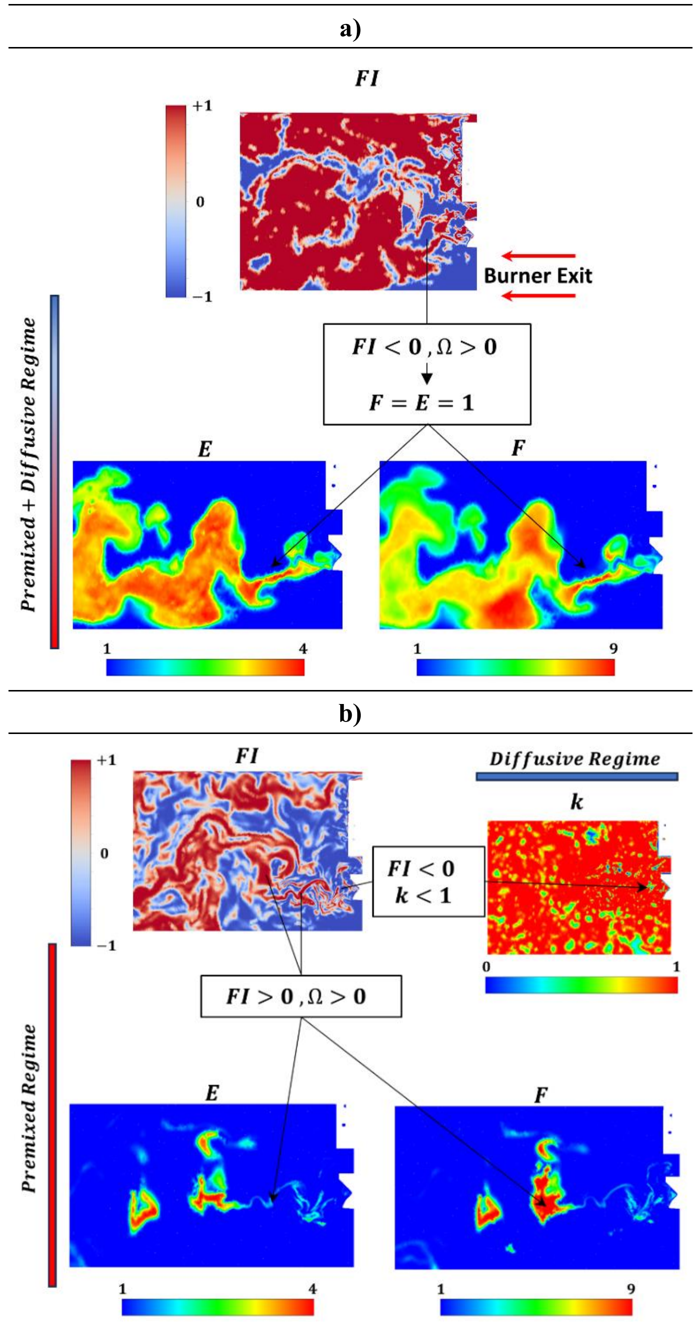

FIGURE 6: CORRELATION BETWEEN FI, E, AND F FOR THE TFM-FR APPROACH (a) AND BETWEEN FI, E, F, AND K FOR THE TFM-EDC CLOSURE (b)

length seems to be much better aligned with the experiments: the total envelope of the numerical HRR is quite close to the one recorded during the tests.

Figure 4 helps to shed light on these results showing the combustion regime at the main locations of the primary zone for both the numerical approaches, reporting the time averaged field of the product between the HRR and the FI (mathematically, the premixed regime is identified by positive values). It can be noticed that the $TFM - EDC$ approach is characterized by an intense diffusive regime not only right downstream the pilot jets but also in the core of the domain and close to the burner exit where it interacts with the premixed flow coming from the swirler. Also, the cross sections reported in the figure (Plane A-A) reveal that the diffusive regime is dominant for the $TFM - EDC$ compared to the $TFM - FR$. The enhanced lift-off of the pilots in the former case can lead the diffusive flame to interact more intensely with the premixed flow coming from the burner: as a result, the oxidation of the main can proceed also in the non-premixed regime favoring the shortening of the total flame length. Figure 4 reports also the instantaneous contour plot of the methane consumption rate in a magnified view of the region immediately after the pilots. From these contour plots it can be appreciated how different the pilot-flame structure is when the TCI is included.

One of the main consequences of the different flame stabilization mechanism concerns the thermal field. Figure 5 shows the scatter plot of the time average temperature as a function of the mean mixture fraction considering the cells belonging to the symmetry plane of the flame tube, from the burner exit up to 6 equivalent burner exit diameters. Each point is colored by k for the $TFM - EDC$ closure and by E for $TFM - FR$. It can be observed that the points across the stoichiometric value identifying the pilot regions have a gradual temperature rise with k in the former case up to a maximum value that is instead exceeded in the latter. This can be also seen in the corresponding contour plots of the temperature reported in Figure 5: when the TCI is neglected the temperature reaches the peak right downstream the pilot injection.

From a purely numerical point of view, Figure 6 lets the reader visualize how the two combustion models work. Adopting the $TFM - FR$ closure, both combustion regimes can be described through E and F: their values are simply set to 1 in case of negative FI value (and $\Omega > 0$). More importantly, Figure 6-b reports the map of k through which the non-premixed regime is modelled along the $TFM - EDC$. The instantaneous contour of such quantity reveals that the reactivity is locally lowered ($k < 1$) in those cells around the pilot jet where the flame index is negative. This enhances the flame lift-off with the benefits in terms of flame morphology prediction described above. Indeed, the reduction in reactivity in the diffusive regime allows for more fuel to survive the mixing process. As a result, the premixed region becomes richer, shifting the heat release peak downstream to align with experimental data. This increased global reactivity also leads to a shorter flame.

4.2. Velocity Field and Mixing Characterization

As the last validation step, the velocity fields in reactive conditions coming from the two simulations are compared with the corresponding experimental PIV. Unfortunately, there are some uncertainties about the quantity of seeding to be used to fully characterize the velocity field performing the PIV. It has been found that the employed quantity is not fully able to provide accurate results far from the burner exit. For this reason, the contour plots reported in Figure 7 show only an axial extension inside the primary zone of about 2.5 times the burner exit diameter, D.

It is found that the two simulations are affected by negligible differences, meaning that the flow field is marginally impacted by the flame topology discrepancies discussed in the previous paragraph. This is demonstrated also by the circumferentially averaged profile of the time averaged axial velocity extracted at the distance D from the dome plate.

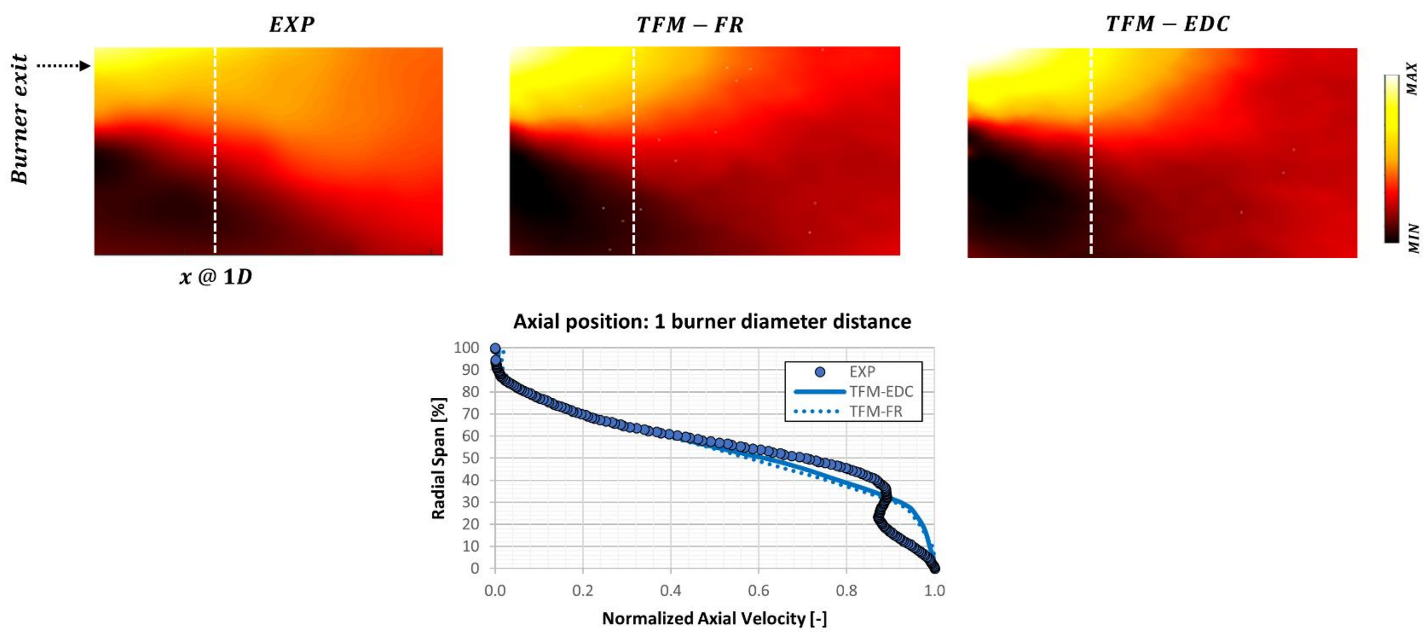

FIGURE 7: VELOCITY FIELD IN THE PRIMARY ZONE—THE NUMERICAL SIMULATIONS ARE COMPARED WITH THE EXPERIMENTAL DATA FROM THE PIV ACQUIRED INSIDE THE PRIMARY ZONE OF THE FLAME TUBE

Conversely, some differences can be noticed against the experimental velocity field and, more specifically, in the radial span range going from the burner exit (0%) up to about 35%: this is the region where the effect of the shear layer generated by the flow coming out from the burner is dominant. In this region the numerical axial velocity profiles are characterized by a smooth velocity decay, which is not observed in the PIV measurements. Apart from this difference, and considering the experimental uncertainties, the numerical models seem to be sufficiently adequate for the flow field prediction. No additional comparison in terms of radial profile is here presented since the higher the distance from the burner exit, the higher the uncertainty related to the PIV measurements.

5. CONCLUSIONS

In this work, a novel extension of the Thickened Flame Model (TFM) for multi-regime combustion is proposed and compared to the current state-of-the-art TFM hybridization. While both approaches use the TFM to describe the premixed regime, the key difference lies in the treatment of the non-premixed regime. The reference approach neglects turbulence-chemistry interaction (TCI) and relies on the finite-rate (FR) closure, whereas the proposed method incorporates the EDC formulation to model TCI. This choice is driven by the fact that, while DNS-like simulations with adequate mesh resolution experience minimal impact from omitting TCI, in high-Reynolds-number industrial flows with more stringent resolution constraints, neglecting TCI can significantly compromise the accuracy of the numerical solution. Specifically, the FR (no TCI) tends to overestimate the heat release distribution with increasing mesh size, as demonstrated by Cuenot et al. [13]. In contrast, the EDC model, which incorporates a dependence on sub-grid scale quantities, shows weaker sensitivity to mesh resolution, enabling a more accurate reconstruction of the heat release distribution on coarser meshes.

The key findings of this numerical investigation are summarized below:

- High-fidelity simulations were carried out on an industrial burner exhibiting multi-regime combustion, where the non-premixed regime is associated with the pilot fuel line that ensures flame stabilization of the main premixed mixture. The mesh resolution used in the simulations aligns with the standards typically found in industrial applications.
- The comparison with experimental chemiluminescence reveals that the TFM-EDC model has a higher accuracy in predicting not only the flame lift-off associated with the pilot flames but also the shorter flame characterizing the main one.
- When the TCI is not considered, the pilot flame burns quite rapidly avoiding most of the interaction with the main one, whose heat release region results much more elongated. In contrast, with the EDC lowering the local reactivity within the diffusive regime, more fuel survives the mixing process, leading to a richer premixed region and finally shifting the heat release peak downstream to align with experimental data.
- The impact on the thermal field of the different closures has been also discussed, highlighting the influence of the key numerical parameters.
- Additionally, the verification of the different mathematical formulation of the combustion models onto the flow field has been discussed. Regarding the former, small discrepancies emerge in the main shear layer flow prediction when comparing the numerical results with the corresponding PIV.

While this study focused on evaluating the basic formulation of the EDC model within an LES context, the methodology presented can be extended to investigate alternative non-premixed source term models, such as those based on fractal theory or the Partially Stirred Reactor (PaSR). Alternative formulations or extensions of the EDC model for LES will be investigated in future work.

ACKNOWLEDGEMENTS

The project TRANSITION (fuTure hydRogen Assisted gas turbiNeS for effective carbon capTure IntegratiON) has received funding from the European Union’s Horizon Europe research and Innovation programme under the Grant Agreement No 101069665.

Funded by the European Union

Funded by the European Union. Views and opinions expressed are however those of the author(s) only and do not necessarily reflect those of the European Union. Neither the European Union nor the granting authority can be held responsible for them.

REFERENCES

[1] Amerighi M., Andreini A., Reichel T., Tanneberger T., Paschereit C.O, *“LES investigation of a swirl stabilized technically premixed hydrogen flame with FGM and TFM models”*, Applied Thermal Engineering, Volume 247, 2024. https://doi.org/10.1016/j.applthermaleng.2024.122944

[2] Meloni R., Gori S., Andreini A., Nassini P.C. (October 13, 2021). *"CO Emission Modeling in a Heavy Duty Annular Combustor Operating with Natural Gas" J. Eng. Gas Turbines Power*. January 2022; 144(1): 011011. https://doi.org/10.1115/1.4052028

[3] Cerutti M., Giannini N., Ceccherini G., Meloni R., Matoni E., Romano C., Riccio G. *"Dry Low NOx Emissions Operability Enhancement of a Heavy-Duty Gas Turbine by Means of Fuel Burner Design Development and Testing"*. Proceedings of the ASME Turbo Expo 2018: Turbomachinery Technical Conference and Exposition. Volume 4B: Combustion, Fuels, and Emissions. Oslo, Norway. June 11–15, 2018. https://doi.org/10.1115/GT2018-76587

[4] R. Meloni, P.C. Nassini, A. Andreini, *"Model development for the simulation of the hydrogen addition effect onto the NOx emission of an industrial combustor"*, Fuel, Volume 328, 2022, https://doi.org/10.1016/j.fuel.2022.125278

[5] S. Marragou, H. Magnes, A. Aniello, T.F. Guiberti, L. Selle, T. Poinsot, T. Schuller, *"Modeling of H2/air flame stabilization regime above coaxial dual swirl injectors",* Combustion and Flame, Volume 255, 2023, https://doi.org/10.1016/j.combustflame.2023.112908

[6] A. Gruber, O.H.H. Meyer, T. Heggset, B. Wood, A. Ciani, *"Numerical Investigation of Reheat Hydrogen Flames in the Sequential-Combustion Stage of a Heavy-Duty Gas Turbine"*. Proceedings of the ASME Turbo Expo 2024: Turbomachinery Technical Conference and Exposition. Volume 3B: Combustion, Fuels, and Emissions. London, United Kingdom, 2024. https://doi.org/10.1115/GT2024-128966

[7] P.C. Nassini, D. Pampaloni, R. Meloni, A. Andreini, *"Lean blow-out prediction in an industrial gas turbine combustor through a LES-based CFD analysis"*. Combustion and Flame, Volume 229, 2021. https://doi.org/10.1016/j.combustflame.2021.02.037

[8] Meloni, R., Andreini, A., and Nassini, P. C. (October 13, 2021). *"A Novel Large-Eddy Simulation-Based Process for NO_x Emission Assessment in a Premixed Swirl Stabilized Combustion System". ASME.* J. Eng. Gas Turbines Power. January 2022; 144(1). https://doi.org/10.1115/1.4052027

[9] Dillon S., Mercier R., Fiorina B., *"A new filtered tabulated chemistry model for multi-regime combustion: A priori validation on a laminar triple flame"*. Proceedings of the Combustion Institute, Volume 40, Issues 1–4, 2024. https://doi.org/10.1016/j.proci.2024.105301

[10] Magnussen B., *"On the structure of turbulence and a generalized eddy dissipation concept for chemical reaction in turbulent flow"*. 19th Aerospace Sciences Meeting, 1981, St. Louis, MO, USA https://doi.org/10.2514/6.1981-42

[11] Castellani S., Meloni R., Orsino S., Ansari N., Yadav R., Bessette D., Boxx I., Andreini A.. *"High-fidelity H_2–CH_4 jet in crossflow modelling with a flame index-controlled artificially thickened flame model"*, International Journal of Hydrogen Energy, Volume 48, Issue 90, 2023. https://doi.org/10.1016/j.ijhydene.2023.05.210

[12] Agostinelli P.W., Laera D., Chterev I., Boxx I., Gicquel L., Poinsot T., *"Large eddy simulations of mean pressure and H_2 addition effects on the stabilization and dynamics of a partially-premixed swirled-stabilized methane flame"*, Combustion and Flame, Volume 249, 2023, https://doi.org/10.1016/j.combustflame.2022.112592

[13] Cuenot B., Shum-Kivan F., Blanchard S., *"The thickened flame approach for non-premixed combustion: Principles and implications for turbulent combustion modeling"*. Combustion and Flame, Volume 239, 2022. https://doi.org/10.1016/j.combustflame.2021.111702

[14] G. Lemmi, S. Castellani, P.C. Nassini, A. Picchi, S. Galeotti, R. Becchi, A. Andreini, G. Babazzi, R. Meloni, *"FGM vs ATF: A comparative LES analysis in predicting the flame characteristics of an industrial lean premixed burner for gas turbine applications"*, Fuel Communications, Volume 19, 2024, https://doi.org/10.1016/j.jfueco.2024.100117

[15] Meloni R., Babazzi G., Giannini N., Castellani S., Nassini P.C., Picchi A., Galeotti S., Becchi R., Andreini A. (October 15, 2024). *"Thickened Flame Model Extension for Dual Gas Turbine Combustion: Validation Against Single Cup Atmospheric Test"*. ASME. J. Eng. Gas Turbines Power. March 2025; 147(3): 031019. https://doi.org/10.1115/1.4066511

[16] Aniello A., Laera D., Marragou S., Magnes H., Selle L., Schuller T., Poinsot T., *"Experimental and numerical investigation of two flame stabilization regimes observed in a dual swirl H_2-air coaxial injector"*. Combustion and Flame, Volume 249, 2023, https://doi.org/10.1016/j.combustflame.2022.112595

[17] O. Colin, F. Ducros, D. Veynante, T. Poinsot; *"A thickened flame model for large eddy simulations of turbulent premixed combustion"*. Physics of Fluids, 1 July 2000; 12 (7): 1843–1863. https://doi.org/10.1063/1.870436

[18] L. Durand, W. Polifke, *"Implementation of the thickened flame model for Large Eddy simulation of turbulent premixed combustion in a commercial solver"*, Proc. ASME Turbo Expo. 2 (2007) 869–878. https://doi.org/10.1115/GT2007-28188

[19] Bilger, R.W., Masri, A. R., Yip, B., and Long, M. B., 1990. *"An Atlas of QEDR Flame Structures"*, Combustion Science and Technology, 72(4-6), pp. 137‑155. ttps://doi.org/10.1080/00102209008951645

[20] *Chemical-Kinetic Mechanisms for Combustion Applications*, , San Diego Mechanism web page, Mechanical and Aerospace Engineering (Combustion Research), University of California at San Diego (http://combustion.ucsd.edu)

[21] Meloni R., Orsino S., Ansari N., Yadav R., Bessette D., Castellani S., Nassini P.C., Andreini A., Boxx I. *"Partially Premixed Hydrogen-Methane Flame Simulations at Relevant Gas Turbine Conditions with*

a Thickened Flame Model Enhancement". Proceedings of the ASME Turbo Expo 2023: Turbomachinery Technical Conference and Exposition. Volume 3 *Combustion*, Fuels, and Emissions. Boston, Massachusetts, USA. 2023. https://doi.org/10.1115/GT2023-102427

[22] D.G. Goodwin, R.L. Speth, H.K. Moat, B.W. Weber, *"Cantera: An object-oriented software toolkit for chemical kinetics, thermodynamics, and transport processes"*, 2018.

[23] G. Wang, M. Boileau, D. Veynante, *"Implementation of a dynamic thickened flame model for large eddy simulations of turbulent premixed combustion"*, Combustion and Flame, Volume 158, Issue 11, 2011. https://doi.org/10.1016/j.combustflame.2011.04.008

[24] M. Farokhi, M. Birouk, "*A comprehensive assessment of fractal wrinkling/eddy dissipation based combustion model for simulating conventional turbulent premixed and non-premixed flames*", Combustion Theory and Modeling, Volume 25, Issue 2, 2021. https://doi.org/10.1080/13647830.2020.1854349

[25] I. S. Ertesvag, "Analysis of some recently proposed modifications to the eddy dissipation concept (EDC)", Combustion Science and Technology, Volume 192, 2018. https://doi.org/10.1080/00102202.2019.1611565

[26] Babazzi G., Galeotti S., Picchi A., Becchi R., Cerutti M., Andreini A. "Combustion Diagnostics and Emissions Measurements of a Novel Low NO_x Burner for Industrial Gas Turbine Operated with CO_2 Diluted Methane/Air Mixtures". *J. Eng. Gas Turbines Power*. July 2024; 146(7). https://doi.org/10.1115/1.4064266